

DOI:10.5937/jaes0-36140

Paper number: 20(2022)3, 983, 765-777

www.engineeringscience.rs \* ISSN 1451-4117 \* Vol.20, No 3, 2022

# A NUMERICAL STUDY OF THE COMPARISON OF NORMAL CONCRETE AND LIGHT WEIGHT CONCRETE EXTERIOR BEAM-COLUMN JOINTS BEHAVIOR TO CYCLIC LATERAL LOADS

Siti Aisyah Nurjannah\*, Saloma, Arie Putra Usman, M. Lindung P. P. Wibowo

Civil Engineering Department, Faculty of Engineering, Universitas Sriwijaya, Jl, Indralaya, Indonesia

\*sitiaisyahn@ft.unsri.ac.id

*This paper presents a numerical analysis of the exterior Beam-Column Joints (BCJ) in resisting a combination of constant axial and lateral cyclic loads. The materials used in this study were Normal Concrete (NC) and Light Weight Concrete (LWC). Light Weight Concrete has been commonly used to reduce the mass of buildings and minimize the structural damages due to earthquakes. A numerical model of exterior BCJ using NC materials was verified using experimental data from the previous research. Then, these models of exterior BCJ using NC and LWC materials were analyzed to obtain the performance. This study aimed to elaborate on the LWC as materials of structures to resist earthquake loads. The performance of the exterior BCJ models was analyzed through hysteretic curves, ductility, stiffness degradation, and strength degradation. The analysis results showed that the NC-BCJ model achieved a higher maximum story drift of 5.3% than the LWC-BCJ model of 4.5%. NC-BCJ model reached higher maximum lateral forces of 40.58 kN and 40.51 kN under push and pull loads, compared with the LWC-BCJ model of 27.83 kN and 32.40 kN. The exterior NC-BCJ model satisfied the strength criteria in the ACI 374.1-19 with a ratio of 1.0 under push and pull loads. Despite the lower maximum lateral forces achieved by the LWC-BCJ model than NC-BCJ, it satisfied this criterion with ratios of 0.93 and 0.99 under push and pull loads, respectively. Both NC-BCJ and LWC-BCJ models performed moderate ductility of 2.70 and 2.52.*

*Keywords: lightweight concrete, normal concrete, cyclic lateral load, numerical model, ductility, strength, stiffness*

## 1 INTRODUCTION

### 1.1 Literature review

Earthquakes cause many destructions on building structures and influence the safety level of the occupants. Therefore, buildings structures need to be designed to resist seismic loads. In the reinforced concrete structures, the failure on the beam and column joints often occurs due to the distribution of cyclic lateral loads. Then, it requires specific details of reinforcement on the joints and analysis of the behavior. To minimize destruction due to earthquakes, it needs to reduce the mass of buildings by using lightweight materials. One of these materials is Light Weight Concrete (LWC), with a bulk density of 500-800 kg/m<sup>3</sup> [1,2]. This study aims to analyze the performance of the exterior Beam-Column Joints (BCJ) using Normal Concrete (NC) and Light Weight Concrete materials in resisting a combination of constant axial and lateral cyclic loads using a numerical program.

In ensuring the lateral stability of the structure, it needs to provide the adequate performance of the exterior and interior BCJ. Every exterior BCJ needs to be considered as it is more critical than the interior BCJ due to only one beam to perform the energy dissipation in resisting lateral loads. In the previous study, the research was conducted through an experimental program on several exterior BCJ specimens using Normal Concrete and High Strength Concrete (HPC) under a combination of constant axial and lateral cyclic loads [3]. The specimens achieved adequate performance in resisting loads. The hysteretic curves showed sufficient energy dissipation, strength, and stiffness. Two of six specimens performed pinching behavior because of the bar slip in the joints. It was due to a column to beam moment capacity ratio (MR) of 1.2, while the four un-pinching specimens' MRS were 2.1 and 2.3.

There are many ways for researchers to provide better performance of exterior BCJ behavior. One of them used mechanical and forging splices of the bars [4]. Compared with the conventional bars, the exterior BCJs with forged bars on the beams showed more ductile, higher energy dissipation, and higher stiffness under lateral cyclic loads. This behavior was due to the larger bar area in the splices that provided higher nominal capacity in resisting loads. Using a certain number of Grade 600 MPa bars on the beam as a longitudinal reinforcement of an exterior BCJ resulted in decreased shear deformation and shear crack width [5]. The total area of the Grade 600 MPa bars needed to be considered wisely because the principal strain increased in line with the Grade of the bar. The higher compressive strength also decreased joint shear deformation and shear crack width. Beydokhty, et al. [6] investigated the behavior of cyclic loads of exterior BCJ specimens. The cyclic load tests were carried out until the drift reached 5%. The carbon-fiber-reinforced plastic (C-FRP) sheets were used to improve the seismic capacity and stiffness of the specimens. Bond slip often occurs at the junction between normal concrete and reinforcing steel, thereby reducing the performance of the exterior BCJ in resisting lateral cyclic loads. The use of high-strength steel fiber reinforced concrete (SFRHSC) and X-shaped reinforcement in the joint region had been

proposed to improve joint performance [7]. The test results showed that the combination of SFRHSC and X-shaped reinforcement in the joint region significantly increased the loading capacity and energy dissipation. The HPC of 70 MPa and Grade 600 MPa bars also were used in the research [3]. Three exterior BCJ specimens used a reduced number of Grade 600 longitudinal reinforcement bars to achieve yield stress and provide the same proportional nominal capacity as the other three exterior BCJ specimens using Grade 420 MPa bars. The results showed that the three exterior BCJ specimens that used Grade 420 MPa longitudinal reinforcement bars achieved higher energy dissipation than the other exterior BCJ specimens that used a reduced number of Grade 600 MPa longitudinal reinforcement bars. This behavior was due to the reduced number of Grade 600 MPa longitudinal reinforcement bars providing less MR than decreased the lateral loads faster than the BCJ specimens that used Grade 400 MPa longitudinal reinforcement bars. Despite this behavior, the exterior BCJ specimen with concrete compressive strength of 32 MPa and a reduced number of Grade 600 longitudinal reinforcement bars or Reduced High Strength (RHS)-30 still showed adequate stiffness and strength. It satisfied all the stability criteria [8].

### 1.2 Research significant

The performance of BCJ with dimension and reinforcement details using Normal Concrete and Light Weight Concrete was investigated. In this study, the RHS-30 specimen [3] was modeled using a nonlinear finite element program, namely ANSYS. The RHS-30 was renamed Normal Concrete-Beam-Column Joint (NC-BCJ). This paper presented numeric models to provide further information on strength, stiffness, load, deformation, stress distribution, energy dissipation, and ductility. The same analysis procedure was also applied to the exterior BCJ numerical model using LWC materials (LWC-BCJ). Although the performance of the LWC-BCJ model was under the NC-BCJ, it showed sufficient strength, stiffness, energy dissipation, and ductility. In this study, the compressive strengths of NC and LWC are 32 MPa and 27.9 MPa, respectively, while the modulus elasticities of NC and LWC are 26,587 MPa and 15,955 MPa, respectively.

### 1.3 Normal Concrete and Light Weight Concrete

There are three stages in the stress-strain curve of the Normal Concrete materials: the linear elastic, inelastic, and stain-softening or post-peak response [9]. The curve approaches 40% of the concrete compressive strength ( $f_c$ ) in the linear elastic stage. Then, it increases to more than 40% of the concrete compressive strength and forms an ascending branch of the strain-stress curve. This change causes cracks and makes the stress-strain curve turns into an inelastic stage until the compressive strength is achieved. After the curve reaches the compressive strength in the descending branch, the cracks propagate, form patterns, and separate aggregates from the cement matrix. Light Weight Concrete uses an expanding agent to increase the volume of the concrete mixture and reduce the dead load [10]. The LWC density ranges from 650 kg/m<sup>3</sup> to 1850 kg/m<sup>3</sup> compared to 1800 kg/m<sup>3</sup> and 2400 kg/m<sup>3</sup> for conventional brick and concrete. Despite millions of tiny air-filled cells, it is solid and durable. This type of concrete is lighter than conventional and has low thermal conductivity [11].

## 2 MATERIALS AND METHODS

### 2.1 Materials

The compressive strengths of NC and LWC in this study were 32 MPa [3] and 27,9 MPa [12], while the elastic modulus values were 26,587 MPa [3] and 15,955 MPa [12], the mass density were 2200 [3] kg/m<sup>3</sup> and 1702.5 kg/m<sup>3</sup> [12], respectively. The bar properties are as shown in Table 1. The stress-strain curves of NC and LWC are shown in Fig. 1.

Table 9. Properties of bar reinforcement

Diameter [mm]	Grade [MPa]	Yield Strength [MPa]	Elastic Modulus [MPa]
12	600	604	201.4
10	600	602	201.6
8	420	425	205.9

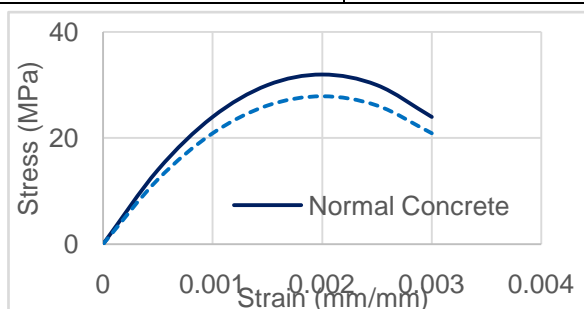


Fig. 15. Stress-strain curves of Light Weight Concrete and Normal Concrete [3,12].

## 2.2 Finite Element Method

The Finite Element Method (FEM) was used in modeling the exterior Beam-Column Joints using Normal Concrete and Light Weight Concrete materials. In this study, a FEM program called ANSYS was used for numerical modeling of exterior Beam-Column Joints under a combination of constant axial and lateral cyclic loads. The core of the FEM is to mesh an object into several smaller parts with a finite number of elements connected by nodes. The complete sequences in using ANSYS software are problem specifications, defining materials, problem descriptions, building geometry, generating the mesh, attribute mesh to model, boundary conditions, obtaining solutions, and review results [13].

### 2.3 Concrete, steel bar, and steel plate elements

SOLID65 is an element that provides properties as concrete. This element can behave by compression, tension, and crack propagation of concrete, as shown in Fig. 2. Each SOLID65 element has eight nodes that resemble a cube or block and is used with or without reinforcement. LINK180 is an element that represents trusses, curved cables, and links. These two nodes of LINK180 behave like steel bar reinforcement. This element has two nodes and is presented in Fig. 3. SOLID45 is an element that can compress and tension but not crack. Each element has eight nodes and is shown in Fig. 4. Because of this behavior, SOLID45 is suitable to represent steel plates in numerical modeling. The properties of all these three types of elements need to be described in the input of the ANSYS software, such as compressive, yield, and ultimate strengths, modulus elasticities, and strain-stress correlation [14].

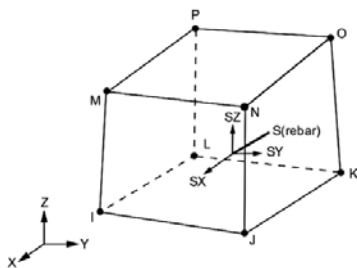


Fig. 2.SOLID65 element

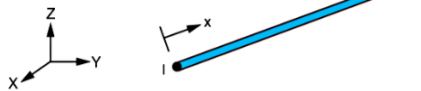


Fig. 3.LINK180 element

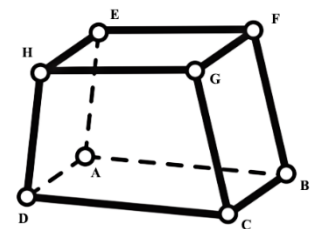


Fig. 4.SOLID45 element

## 2.4 Meshing

The concrete materials of the exterior BCJ have meshed into separated discrete elements of SOLID65. This element could perform concrete properties and behavior, as is shown in Fig. 5. The LINK180 elements were used to model the reinforcement bars and performed axial forces, as shown in Fig. 6.

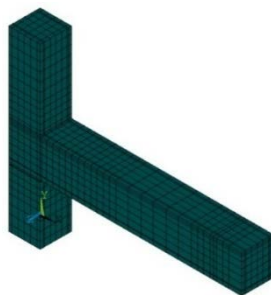


Fig. 5.SOLID65 of concrete model

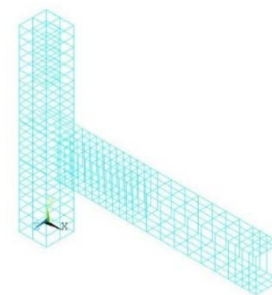


Fig. 6.LINK180 of steel bar model

## 2.5 The nonlinear equation for problem-solving

Eq. (1) is commonly used to solve the linear load problem.

$$[K]\{u\} = \{F^w\} \quad (1)$$

where  $[K]$  is a stiffness matrix, while  $\{u\}$  and  $\{F^w\}$  are the degree of freedom and force of working load vectors, respectively. The numerical model needs the Newton-Raphson iteration process. The incremental equilibrium is expressed in Eqs. (2) and (3).

$$[[K_i^S]\{\Delta u_i\} = \{F^w\} - \{F_i^{nw}\} \quad (2)$$

$$\{u_{i+1}\} = \{u_i\} + \{\Delta u_i\} \quad (3)$$

where  $[K_i^S]$ , is the structural stiffness matrix, while  $\{u_i\}$  and  $\{F_i^{nw}\}$  are degrees of freedom and working load vectors, respectively. The iteration of Eq. (2) is needed to obtain the solution using these steps:

- The value of  $\{u_o\}$  is assumed. It is commonly obtained from the solution of the previous iteration step. Then, for the first iteration:  $\{u_o\} = \{0\}$
- Build the  $[K_i^S]$  matrix,  $\{F_i^{nw}\}$  from confirmed  $\{u_i\}$ .
- Determine  $\{\Delta u_i\}$ .
- Add  $\{\Delta u_i\}$  to  $\{u_i\}$  to obtain  $\{u_{i+1}\}$

## 2.6 Model of specimens

The data for numerical modeling of BCJs included the dimension, reinforcement details, and Normal Concrete properties from the previous study [3]. The properties of LWC materials were based on research by Ramadhanty [12]. Each BCJ consisted of a column and a beam. The dimensions of the column section were 250 mm x 250 mm; the longitudinal and stirrup reinforcement bars of  $\phi 12$  and  $\phi 8$ , respectively. The beam section dimensions were 300 mm x 250 mm with longitudinal and stirrup reinforcement bars of  $\phi 10$  and  $\phi 8$ , respectively. The loading history was referred to the code [8] as shown in Fig. 7.

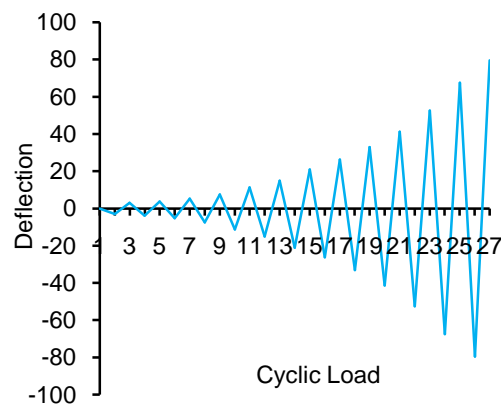


Fig. 7. Loading history

The loading cycle was repeated three times in each drift ratio. The three-cycle loads were modeled numerically with a specific value deflection control (based on loading history [8]) resulting in the same hysteretic curves. The program output is three overlapping hysteretic curves. The output of the hysteretic curves is equal to the load of one cycle's output. This has been done by the author in the previous studies [15,16] and the results were the same as other researcher conducted [17]. Then, the modeling of the cycle was simplified. There was only one cycle in each drift ratio and no relaxation cycle. This single cycle loading produces the same results as three cycles loading in each drift ratio. A combination of constant axial and cyclic lateral loads was applied to the NC-BCJ and LWC-BCJ models. There was one cycle of lateral load in each story drift while the code [8] were suggested three times. The simplification of load modeling was based on the stiffness behavior of the models where the second and third cycles produced the same hysteretic curve with the first cycle in each drift ratio [15]. However, the numerical models satisfied the accuracy by less than 10% [18]. In the numerical modeling, the cracked concrete elements are not considered to the contribution of strength and stiffness. It is different in the experiments, where the cracked concrete still contributes strength and stiffness under loadings [19]. This behavior makes the hysteretic curve areas of numerical models are less than in the experiments. The numerical program's boundary conditions were similar to the laboratory setup to ensure that the models behaved as the specimens.

## 2.7 Reinforcement details

The dimension and reinforcement details of the Beam-Column Joint(BCJ) specimen were based on the previous study [3], as is shown in Fig. 8 (redrawn). It was designed referring to ACI 318-19 [20]. The number of the Grade 600 MPa steel bars in the specimen were intended to provide an equal flexural strength of the Grade 420 MPa bars. In this study, these details were modeled for numerical analysis.

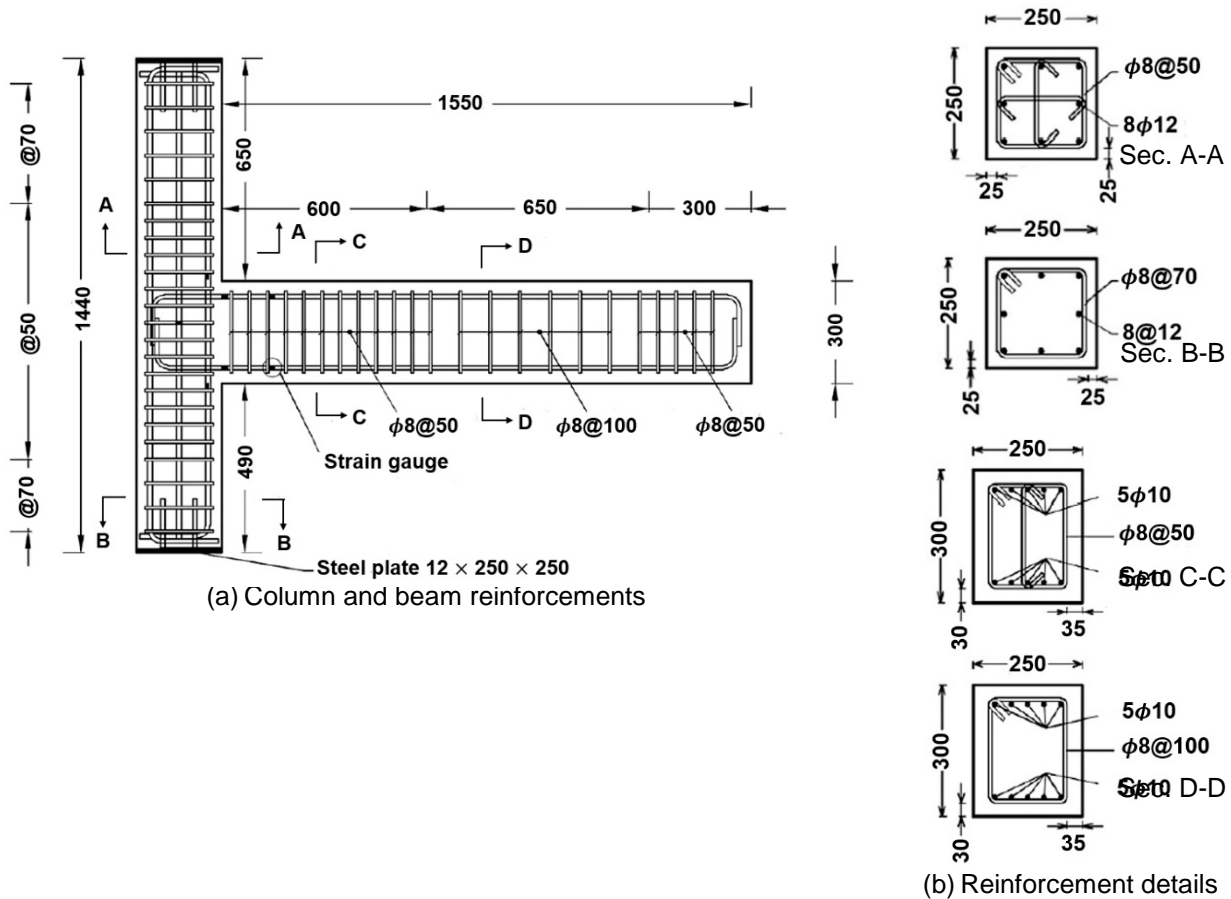


Fig. 8. Dimension and reinforcement details of the BCJ and sections (in mm; redrawn)[3]

### 3 RESULTS AND DISCUSSION

#### 3.1 Hysteresis curves of experimental and numerical model of the Normal Concrete Beam-Column Joints

The numerical modeling was conducted to analyze the hysteretic behavior of the exterior Beam-Column Joints. The specimen was placed on the loading frame and resisted loads from the axial and lateral hydraulic jacks in the previous study [3]. As with the experimental program, the observed lateral deflection was in the side of the top column using a Linear Variable Displacement Transducer (LVDT). The lateral forces were observed in the same location and recorded using a load cell. All these data were transferred into a data logger. The result of the numerical analysis was the hysteresis curve. This curve was compared with the experimental results, as is shown in Fig. 9. In this figure, there are three hysteretic curves. The blue and red curves represent the previous study's experimental and analytical results [3]. The black curve represents the numerical analysis using the ANSYS program. The numerical and experimental results are compared in Tables 2 and 3. The experiment and numerical model results examined maximum lateral forces and displacement in the push and pull loading directions. The numerical modeling satisfied the accuracy as the differences between lateral loads and displacements are less than 10% [18]. In the numerical model and experiment, the maximum lateral loads in the push and pull loading directions occurred in the same story drifts of 4.5% and 3.5%, respectively. The maximum story drifts achieved by the numerical model and experiment were also the same, which were 5.3% both in the push and pull loading directions. It showed that the hysteretic curve of the numerical model of NC-BCJ was similar with the experimental results. The specimen and model of NC-BCJ achieved a maximum story drift of 5.3% exceeded the required 3.50% story drift in the code [8]. This strength criteria in this code regulate the ratio of lateral load in story drift of 3.5% to the maximum load is at least 0.75. Because both the specimen and model of NC-BCJ maximum loads occurred in the higher story drift of 3.5%, they satisfied the strength criteria under push and pull loading directions.

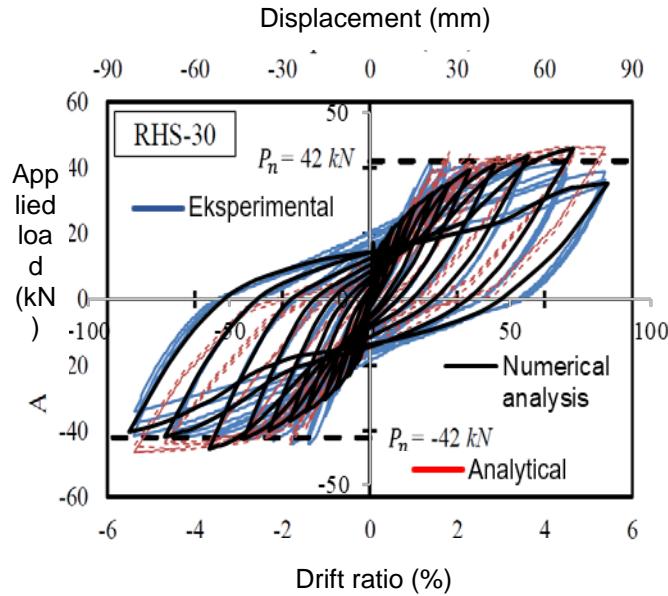


Fig. 9. Hysteretic curves of the numerical analysis and experiment

Table 2. Lateral forces of the numerical model and experimental of NC-BCJ

The direction of lateral force loading	Maximum lateral force [kN]			Difference of force of numeric model to experiment [%]
	NC-BCJ Numerical model	NC-BCJ Experiment	NC-BCJ Analytical [3]	
Push	40.58	41.49	45	2.19
Pull	40.51	43.97	44	7.87

Table 3. Lateral displacement of the numerical model and experimental of NC-BCJ

The direction of lateral force loading	Deflection [mm]			Difference of deflection on the models [%]	Drift ratio at max. load [%]
	NC-BCJ Numerical model	NC-BCJ Experiment	NC-BCJ Analytical [3]		
Push	72.33	67.5	70	7.15	4.5
Pull	57.08	52.5	68	8.73	3.5

### 3.2 Hysteresis curves of Normal Concrete and Light Weight Concrete Beam-Column Joints models

The hysteresis curve is a loading and unloading loads and displacements correlation that describes the response time history of a structural element due to a cyclic load [15]. The hysteresis curves of Normal Concrete and Light Weight Concrete numerical analysis are shown in Figs. 10 and 11. The pull loading was applied and followed by the push loading in each cycle. Some concrete elements cracked after resisting pull loading in several story drifts due to exceeded compressive loads. Then, these elements were not considered in the stiffness matrices and resulted in decreased strength under push loading [16,17]. The resume of maximum achieved story drifts of the experiment, as well as NC-BCJ and LWC-BCJ numerical models, are shown in Table 4. The NC-BCJ numerical model maximum lateral loads in the push and pull loadings occurred in the story drifts of 4.5% and 3.5%, respectively, while the ultimate condition achieved in story drifts of 5.3%. This condition made the model satisfy the acceptance criteria of strength that required at least 0.75 of the maximum lateral force in the story drift of 3.5% [8]. Table 5 shows the maximum lateral forces and deflection that LWC-BCJ numerical model achieved. It reached an ultimate condition in story drift 3.5%, both in the push and pull loading directions. Based on the compression strength, the material of LWC reduced the capacity in resisting maximum load and maximum deformation [21,22] compared to NC material. However, the LWC-BCJ satisfied the stability criteria in the code [8] requiring lateral force in the story drift of 3.5%, which was not less than 0.75 of the maximum lateral force. This behavior is shown in Table 6. Even the ultimate to the maximum lateral force ratios were more than 0.75 under push and pull loadings, as in Table 7. It indicated that the Light Weight Concrete could resist cyclic lateral loads until story drift of 4.5%.

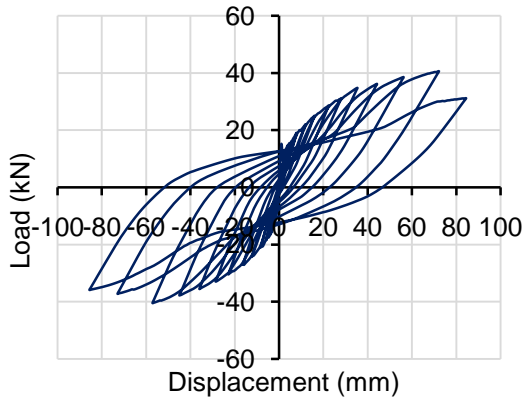


Fig.10. Normal concrete hysteresis curve

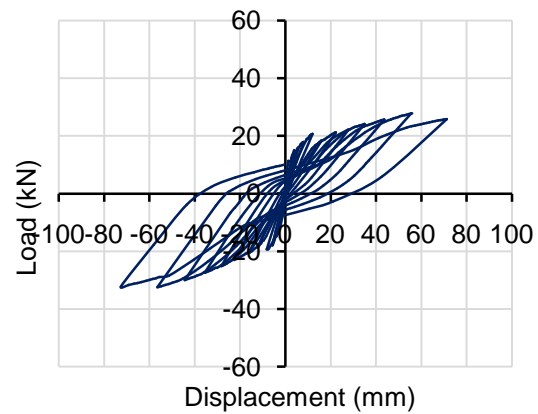


Fig.11. LWC hysteresis curve

Table 4. Maximum drift ratio achieved

The direction of lateral force loading	Drift ratio [%]			
	NC-BCJ Experiment	NC-BCJ Analytical [3]	NC-BCJ numerical model	LWC-BCJ numerical model
Push	5.3	5.3	5.3	4.5
Pull	5.3	5.3	5.3	4.5

Table 5. Lateral forces and displacement of the numerical model of LWC-BCJ

The direction of lateral force loading	LWC-BCJ Numerical model		Drift ratio [%]
	Maximum lateral force [kN]	Deflection [mm]	
Push	27.83	55.60	3.5
Pull	32.40	56.45	3.5

Table 6. Lateral forces of the numerical model of LWC-BCJ in story drift of 3.5%

The direction of lateral force loading	LWC-BCJ numerical model			
	Maximum lateral force [kN]	Drift ratio [%] in the maximum lateral force	Lateral force [kN] in story drift 3.5%	At least 0.75 of max. lateral force
	(1)	(2)	(3)	(4) = (3)/(1)
Push	27.83	3.5	27.83	1.00
Pull	32.40	3.5	32.40	1.00

Table 7. Lateral forces of the numerical model of LWC-BCJ in story drifts of 4.5% and 3.5%

The direction of lateral force loading	LWC-BCJ numerical model			
	Maximum lateral force [kN]	Drift ratio [%] in the maximum lateral force	Lateral force [kN] in story drift 4.5% (ultimate)	The ratio of ultimate to the maximum lateral force
	(1)	(2)	(3)	(4) = (3)/(1)
Push	27.83	3.5	25.87	0.93
Pull	32.40	3.5	32.18	0.99

### 3.3 Stress contour and maximum story drifts

The stress contours of the NC-BCJ and LWC-BCJ models under cyclic lateral push loading are in Figs. 12 and 13, while Figs. 14 and 15 show stress contours under pull loads. Figs. 12 and 13 indicate that the highest stress occurred (blue color) at the beam-column connection due to cyclic lateral loads. This behavior is consistent with the results of other studies [23,24]. As the concrete strained, the stress exceeded the compressive and tensile strength

of NC and LWC materials, then caused cracks. Due to lateral cyclic loading, the steel bars also were strained and exceeded the yield stress. In Fig. 12, the NC-BCJ model maximum compression stress was 33.89 MPa. It was shown in the green color on the beam plastic hinge. It was higher than the concrete compressive strength of 32 MPa, resulting in significant damage. The high compressive stress was concentrated on the beam plastic hinge as the same with other studies [23,24] in the yellow color and spread to 45 cm from the column surface. In the front and rear sides of the beam and column plastic hinges and joint, the compressive stress ranged from 2.78 to 10.56 MPa. The column plastic hinges' maximum compressive stress ranged from 10.56 to 18.33 MPa near the beam, about 30 cm in the yellow color. The constant axial load on the top of the column influenced the support, making the compressive stress of 10.56 to 18.33 MPa. The LWC-BCJ model in Fig. 13 showed similar behavior. It achieved maximum compression stress of 33.89 MPa and spread only in small areas on the beam plastic hinge. There was also compression stress that ranged between 10.56 to 18.33 MPa until 40 cm from the column surface in yellow color, but the area was smaller than in NC-BCJ. The compressive stress of 2.78 to 10.56 MPa also occurred on beam and column plastic hinges and joints in smaller areas. This smaller area indicated that LWC material influenced the LWC-BCJ to achieve lower ultimate stress than NC-BCJ. It was due to the concrete compression strength of LWC that was lower than NC material [21,22]. The compression stress at the column support due to the constant axial load also occurred in smaller areas than NC-BCJ. The maximum story drift caused these differences achieved, where the NC-BCJ and LWC-BCJ ultimate conditions occurred in the story drifts of 5.3% and 4.5%, respectively. Then, the LWC-BCJ compression stress was lower and only spread in small areas compared with the NC-BCJ. In Fig. 14, the NC-BCJ model achieved the maximum compression stress at the end of the beam. The end of the beam represented an inflection point and was constrained by two steel plates on the top and the bottom. Then it resisted the higher compression stress than other beam parts, as shown by the green area of 18.33 to 26.11 MPa. The LWC-BCJ model in Fig. 15 also reached compression stress of 18.33 to 26.11 MPa on the beam inflection point in a smaller area. The compression stress of 2.78 to 10.56 MPa occurred in the NC-BCJ and LWC-BCJ models on the beam plastic hinges and joints. The difference was that the compression stress areas on the LWC-BCJ always were smaller because of the lower compression strength of LWC than NC [21,22].

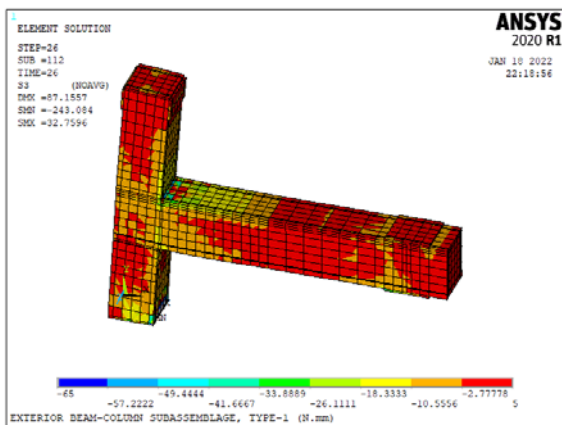


Fig.12. Stress on NC-BCJ in the ultimate condition under cyclic lateral push loading achieved a maximum story drift of 5.3%

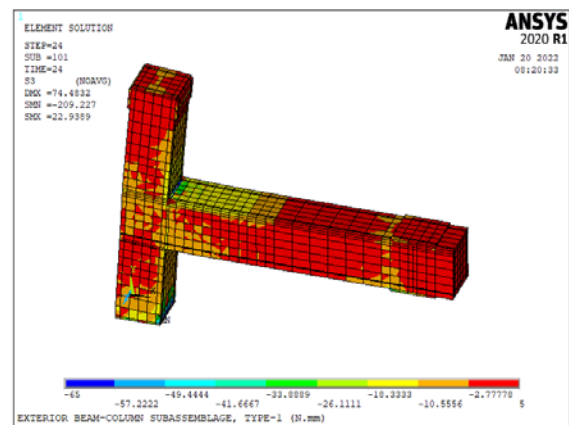


Fig.13. Stress on LWC-BCJ in the ultimate condition under cyclic lateral push loading achieved a maximum story drift of 4.5%

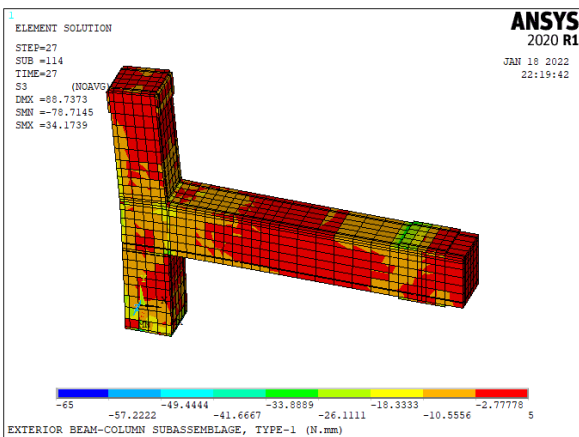


Fig.14. Stress on NC-BCJ in the ultimate condition under cyclic lateral pull loading achieved a maximum story drift of 5.3%

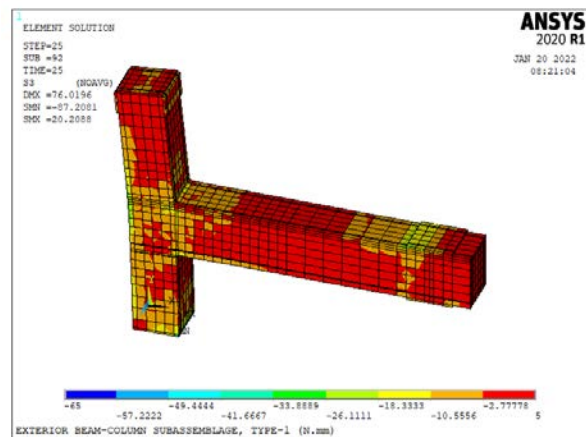


Fig.15. Stress on LWC-BCJ in the ultimate condition under cyclic lateral pull loading achieved a maximum story drift of 4.5%

### 3.4 Displacement ductility

Displacement ductility ( $\mu_\delta$ ) is a ratio of ultimate displacement ( $\delta_u$ ) to the yield displacement ( $\delta_y$ ) and expressed in Eq. (4) [25]. Ductility can deform through the inelastic condition in energy dissipation until the ultimate condition [26,27,28]. The categories of ductility are low (less than 2), moderate (2 to 4), and high (higher than 4) [29]. The determination of yield displacement was based on the method described in a code [29]. Fig. 16 shows the positive post-yielding slope. The dividing line of the force-deflection curve must be determined using an iterative graphical procedure so that the area of the upper and lower curves is relatively equal. The initial stiffness ( $K_i$ ) is in the elastic condition. The effective lateral stiffness ( $K_e$ ) is taken as the shear stiffness calculated at a shear force of 60% of the effective yield strength of the structure. The post-yield slope ( $\alpha$ ) is determined by the dividing line passing through the actual curve at the calculated target displacement. The effective yield strength must not exceed the maximum base shear force at all points along the actual curve. The ultimate displacements are at the end of the backbone curves in Figs. 17 and 18.

$$\mu_\delta = \delta_u / \delta_y \quad (4)$$

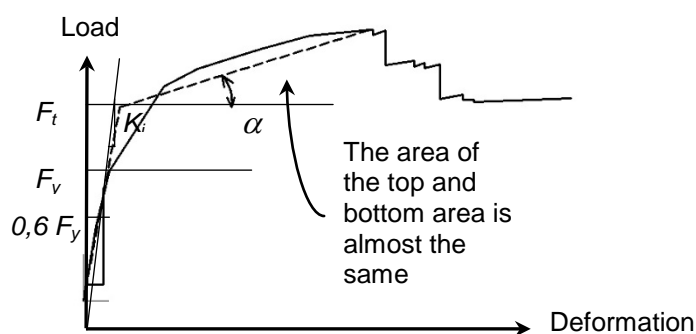


Fig.16.Positive post-yielding slope [29]

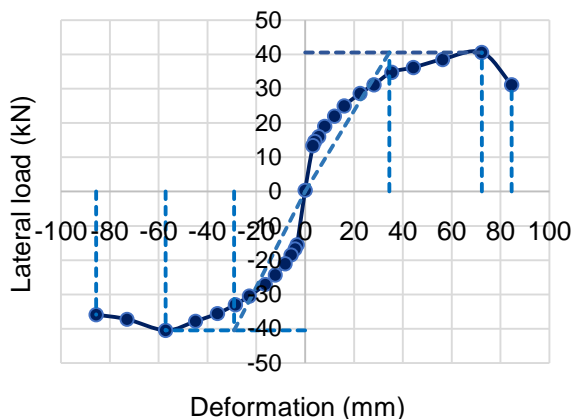


Fig.17.Normal Concrete envelope curve

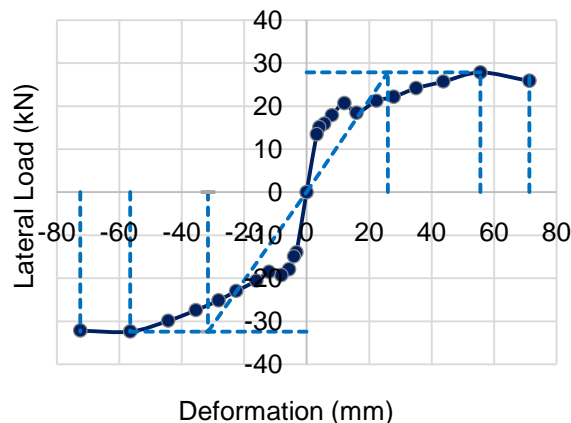


Fig.18.LWC envelope curve

The ductility of the numerical models of NC-BCJ and LWC-BCJ are shown in Tables 8 and 9. The ductility values are 2.70 and 2.52, respectively. These values were close to Dehkordi's experimental results [3], which was 2.25. The ductility values were included in the moderate ductility demand that ranged from 2 to 4 [29]. Structural elements in the form of beam-column joints that behave in moderate ductility can be applied in areas that have the potential for moderate earthquakes [30].

Table 8. Ductility of Normal Concrete Beam-Column Joint based on ANSYS results

Load directions	Ultimate deformation	Yield deformation	Ductility	Average ductility
	$\delta_u$ [mm]	$\delta_y$ [mm]	$\delta_u / \delta_y$	
Push	84.59	34.54	2.45	2.70
Pull	85.56	29.07	2.94	

Table 9. Ductility of Light Weight Concrete Beam-Column Joint based on ANSYS results

Load directions	Ultimate deformation	Yield deformation	Ductility	Average ductility
	$\delta_u$ [mm]	$\delta_y$ [mm]	$\delta_u/\delta_y$	
Push	71.28	25.98	2.74	2.52
Pull	72.48	31.59	2.29	

### 3.5 Stiffness and strength of Normal Concrete and Light Weight Concrete

The stiffness ( $K$ ) is the result of a comparison between the lateral force ( $F$ ) and displacement ( $\delta$ ) in a drift ratio and expressed in Eq. (5) [31]. The correlation between stiffness and drift ratio of the NC-BCJ and LWC-BCJ models was based on the analysis results in the push and pull loading direction are shown in Figs. 19 and 20. Since the story drift of 1.00%, the stiffness degradation occurred on both NC-BCJ and LWC-BCJ models and continued until the end of loading. The stiffness of LWC-BCJ is less than NC-BCJ since story drift of 0.5% and became higher until story drift of 4.5%. The stiffness of NC-BCJ in story drift 5.3% is close to the stiffness of LWC-BCJ in story drift 4.5% due to the higher concrete compressive strength of Normal Concrete than Light Weight Concrete. This behavior of LWC stiffness correlated with the previous studies [21,22].

$$K = \frac{F}{\delta} \quad (5)$$

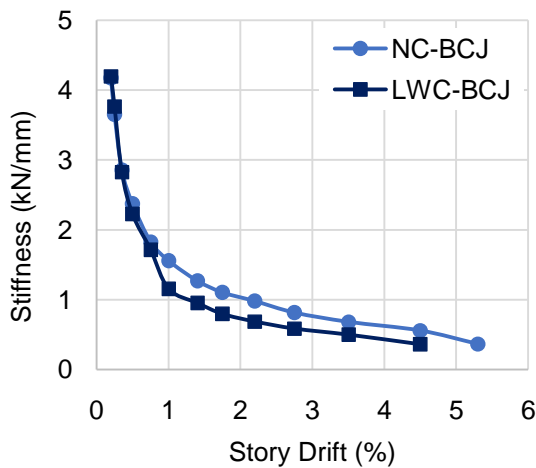


Fig.19. Correlation of the stiffness and story drift of Normal Concrete and Light Weight Concrete Beam-Column Joints under push loading

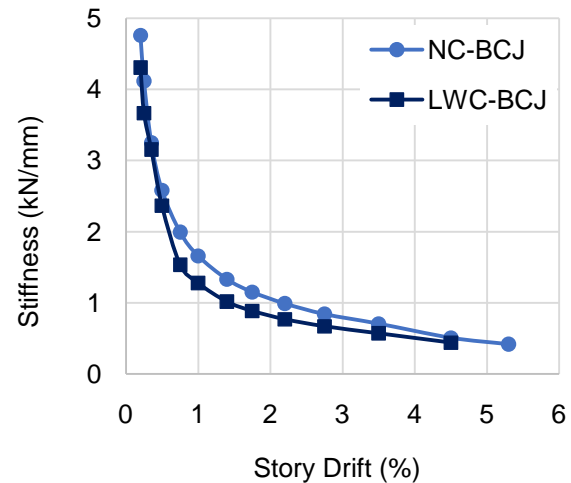


Fig.20. Correlation of the stiffness and story drift of Normal Concrete and Light Weight Concrete Beam-Column Joints under pull loading

Based on Figs. 19 and 20, the percentage of stiffness degradation in the push and pull loading direction of NC-BCJ and LWC-BCJ are presented in Tables 10 and 11, respectively. The NC-BCJ model showed stiffness degradation due to decreased performance after concrete cracks and steel bars yield under cyclic lateral loading. The most significant stiffness degradation cumulative was 91.185% of the initial stiffness in the 5.30% story drift under push and pull loading. The stiffness became lower along with the increased cyclic loading and drift ratio. The LWC-BCJ model also performed the same behavior. The stiffness degradation cumulative became higher and reached 91.353% and 89.691% in story drift of 4.50% under push and pull loadings, respectively. Overall, the stiffness degradation of LWC-BCJ was faster than the NC-BCJ due to the lower concrete compression of LWC material [21,22]. The maximum lateral load in each story drift is called strength. The correlation curve of strength and story drift of NC-BCJ and LWC-BCJ models are shown in Figs. 21 and 22. The strength under push loading increased until story drift of 4.5% with deflection of 72.33 mm and a load of 40.58 kN. Then, the curve descended due to concrete cracks, bar steel yielding until the ultimate point in the story drift of 5.30%. The model showed the different behavior under pull loading, where the curve achieved a maximum load in story drift of 3.50% with deflection of 57.08 mm and a load of 40.51 kN. The ultimate condition occurred in story drift of 5.30% after descending shape of the post-peak load. The LWC-BCJ model performance was different due to the lower concrete compressive strength. It achieved strengths of 27.83 kN and 32.40 kN with deflections of 55.60 mm and 56.45 mm in story drift of 2.75% under push and pull loads, respectively. The LWC-BCJ always performed lower strength and maximum deformation because of the lower compression strength and maximum strain that was showed on Fig. 1 [3,12].

Table 100. Percentage of the Normal Concrete Beam- Column Joint (NC-BCJ) model stiffness degradation

Story drift [%]	Push Loading		Pull Loading	
	Stiffness [kN/mm]	Stiffness Degradation [%]	Stiffness [kN/mm]	Stiffness Degradation [%]
0.20	4.174	0	4.762	0
0.25	3.652	12.506	4.118	13.540
0.35	2.854	31.612	3.250	31.761
0.50	2.374	43.124	2.586	45.699
0.75	1.830	56.147	1.995	58.119
1.00	1.556	62.714	1.664	65.068
1.40	1.270	69.570	1.336	71.956
1.75	1.105	73.533	1.155	75.746
2.20	0.979	76.543	0.992	79.179
2.75	0.816	80.455	0.844	82.288
3.50	0.684	83.607	0.710	85.100
4.50	0.561	86.557	0.511	89.264
5.30	0.368	91.185	0.420	91.185

Table 111. Percentage of the Light Weight Concrete Beam-Column Joint (LWC-BCJ) model stiffness degradation

Story drift [%]	Push Loading		Pull Loading	
	Stiffness [kN/mm]	Stiffness Degradation [%]	Stiffness [kN/mm]	Stiffness Degradation [%]
0.20	4.197	0	4.307	0
0.25	3.768	10.236	3.669	14.801
0.35	2.828	32.630	3.155	26.747
0.50	2.225	46.999	2.370	44.968
0.75	1.713	59.199	1.536	64.325
1.00	1.155	72.482	1.278	70.315
1.40	0.952	77.328	1.018	76.369
1.75	0.796	81.037	0.890	79.324
2.20	0.690	83.562	0.773	82.041
2.75	0.588	85.995	0.674	84.348
3.50	0.501	88.073	0.574	86.674
4.50	0.363	91.353	0.444	89.691

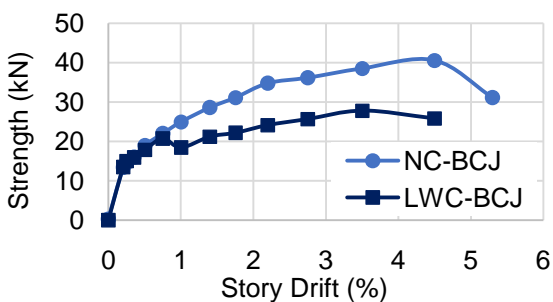


Fig.21. Strength degradation of NC-BCJ and LWC-BCJ under cyclic push loading

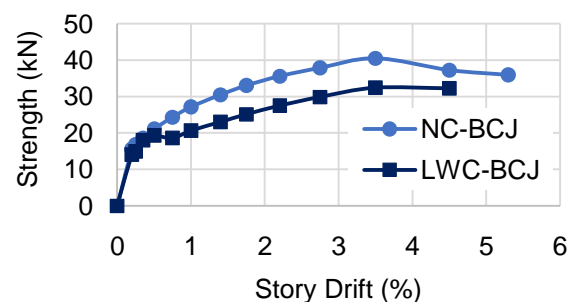


Fig.22. Strength degradation of NC-BCJ and LWC-BCJ under cyclic pull loading

#### 4 CONCLUSIONS

The conclusions based on the numerical study analysis of Normal Concrete and Light Weight Concrete Beam-Column Joints are as follows:

- The numerical model of the Normal Concrete Beam-Column Joint (NC-BCJ) satisfied the error limit since the difference of the lateral loads was less than 10%. It achieved the same story drifts both in the push and pull loading directions. In the next step, the numerical model was applied for determining performance of Light Weight Concrete Beam-Column Joint (LWC-BCJ) and elaborating the LWC as materials of structure in resisting earthquake loads.
- The NC-BCJ specimen and model satisfied the strength criteria based on the code [8] since both the specimen and model of NC-BCJ maximum loads occurred in the higher story drift of 3.5% under push and pull loading directions.
- The LWC-BCJ model showed performance under the NC-BCJ due to less concrete compressive strength. However, they satisfied the strength criteria [8] with ratio of 1.0 for NC-BCJ and 0.93 and 0.99 for LWC-BCJ in the push and pull loading directions, respectively. The maximum story drifts of NC-BCJ and LWC-BCJ models were 5.3% and 4.5%, respectively. It indicated the more ductile behavior of NC-LWC. The higher maximum load of NC-BCJ than LWC-BCJ showed that the concrete compressive strength influenced the BCJs strength. The maximum lateral forces of NC-BCJ and LWC-BCJ under push and pull loads were 40.58 kN and 40.51 kN as well as 27.83 kN and 32.40 kN, respectively.
- For LWC-BCJ model, the strength ratio in story drift of 3.5% to the maximum loads are 1.00 both under push and pull directions. It indicated that Light Weight Concrete could be used as materials of Beam-Column Joints that resist earthquake loads. Even the LWC-BCJ achieved an ultimate story drift of 4.5%, exceeding the required 3.50% story drift.
- The stiffness degradation of LWC-BCJ was faster than LWC-BCJ since story drift of 1% and 0.75% (pull load). This behavior correlated with the strength degradation that occurred in the same story drifts.
- The average ductility of NC-BCJ and LWC-BCJ models ranged in moderate ductility demand based on FEMA 356 [29], which were 2.70 and 2.52, respectively, that could be applied in the moderate earthquake zone.

#### 5 ACKNOWLEDGMENT

The authors would like to thank the support and facilities from Universitas Sriwijaya.

#### 6 REFERENCES

- [1] Sojobi, A. O., Aladegboye, O. J., and Awolusi, T. F. (2018). Green interlocking paving units. *Construction and Building Materials*, vol. 173, pp. 600-614. <https://doi.org/10.1016/j.conbuildmat.2018.04.061>.
- [2] Saloma, Hanafiah, and Urmila, D. (2017). The effect of water binder ratio and fly ash on the properties of foamed concrete, *AIP conference proceedings*, vol. 1903, no. 1, pp. 1-7, <https://doi.org/10.1063/1.5011550>.
- [3] Dehkordi, S. A., Mostofinejad, D., and Alaee, P. (2019). Effects of high-strength reinforcing bars and concrete on seismic behavior of RC beam-column joints, *Engineering Structures*, vol. 183, pp. 702–719, <https://doi.org/10.1016/j.engstruct.2019.01.019>.
- [4] Dabiri, H. and Kheyroddin, A. (2021). An experimental comparison of RC beam-column joints incorporating different splice methods in the beam, *Structures*, vol. 34, pp. 1603–1613, <https://doi.org/10.1016/j.istruc.2021.08.101>.
- [5] Borujerdi, A. S., Mostofinejad, D., Hwang, H. J., and Salimian, M. S. (2021). Evaluation of structural performance for beam-column joints with high-strength materials under cyclic loading using PIV technique, *Journal of Building Engineering*, vol. 44, no. 103283, pp. 1-14, <https://doi.org/10.1016/j.job.2021.103283>.
- [6] Beydokhty, E. Z. and Shariatmadar, H. (2016). Behavior of Damaged Exterior RC Beam-Column Joints Strengthened by CFRP Composites, *Latin American Journal of Solids and Structures*, vol. 13, no. 5, pp. 880-896, <http://dx.doi.org/10.1590/1679-78252258>.
- [7] Zhang, J., Pei, Z., Rong, X., Zhang, X. (2021). Experimental study of HSS-reinforced exterior beam-column joints with different enhancement details. *Engineering Structures*, 246, 113038, pp. 1-19, <https://doi.org/10.1016/j.engstruct.2021.113038>.
- [8] ACI Committee 374. (2019). (reapproved). *ACI 374.1-05 Acceptance Criteria for Moment Frames Based on Structural Testing and Commentary*, American Concrete Institute, Farmington Hills.
- [9] Abdelwahed, B. A. (2020). Review on Reinforced Concrete Beam Column Joint: Role, Modeling and Recent Details. *Journal of Engineering Research*, vol. 8, no. 4, pp. 63-79, <https://doi.org/10.36909/jer.v8i4.8043>.

- [10] Singh, N. T. (2016). Effective uses of Light Weight Concrete. *Journal of Civil Engineering and Environmental Technology*, vol. 3, no. 3, pp. 208-211.
- [11] Li, Z. (2011). *Advanced Concrete Technology*, John Wiley & Sons, Inc., Hoboken, New Jersey.
- [12] Ramadhanty, C. V. (2019). Durability of Lightweight Geopolymer Concrete Against 5% HCl Solution with 14 M NaOH Concentration, Thesis of Undergraduate Program, Civil Engineering Department, Universitas Sriwijaya, Palembang. (Text in Indonesian)
- [13] Kurniawan, F. (2017). Simulation and Analysis of Impact Stress on RIM Truck Wheel with Finite Element Method. Thesis of Undergraduate Program. Institut Teknologi Sepuluh Nopember. Surabaya. (in Indonesian)
- [14] ANSYS v20 R1. (2020). Program manual.
- [15] Budiono, B., Nurjannah, S. A., and Imran, I. (2019). Nonlinear Numerical Modeling of Partially Pre-stressed Beam-column Sub-assemblages Made of Reactive Powder Concrete. *Journal of Engineering and Technological Sciences*, vol. 51, no.1, pp. 28-47, <https://doi.org/10.5614/j.eng.technol.sci.2019.51.1.3>.
- [16] Nurjannah, S. A., Hysteretic Behavior of Partially Pre-stressed Reactive Powder Concrete Beam-column Sub-assemblages, Dissertation, Postgraduate of Civil Engineering Program, Institut Teknologi Bandung, Indonesia, pp. 371, 2016. (Text in Indonesian)
- [17] Kurniawan, R. The Behavior of Reactive Powder Concrete Plate-Column Connection under Gravity and Cyclic Lateral Loads, Doctoral Dissertation, Postgraduate of Civil Engineering Program, Institut Teknologi Bandung, Indonesia, 2015. (Text in Indonesian)
- [18] Badshah, M., Badshah, S., and Jan, S. (2020). Comparison of computational fluid dynamics and fluid structure interaction models for the performance prediction of tidal current turbines. *Journal of Ocean Engineering and Science*, vol. 5, no. 2, pp. 164-172, <https://doi.org/10.1016/j.joes.2019.10.001>.
- [19] Nurjannah, S. A., Budiono, B., and Imran, I. (2020). Influence of Partial Prestressing Ratio On Hysteretic Behavior of Beam Column Subassemblage Using Reactive Powder Concrete Materials, *International Journal of Scientific & Technology Research*, vol. 9, no. 2, pp. 1933-1941.
- [20] ACI Committee 318. (2019). ACI 318R-19. Building Code Requirements for Structural Concrete and Commentary, American Concrete Institute, Farmington Hills.
- [21] Rajeshguna, R., Mariappan, M., Raju, A., and Suguna, K. Cyclic response of high strength fibre reinforced concrete beams with fibre reinforced polymer (FRP) laminates. (2021). *Journal of Materials Research*, vol. 15, pp. 1524-1536, <https://doi.org/10.1016/j.jmrt.2021.08.141>.
- [22] Abdul-Razzaq, K.S., Jebur, S.F., and Mohammed, A.H. (2018). Concrete and Steel Strengths Effect on Deep Beams with Reinforced Struts, *International Journal of Applied Engineering Research*, vol. 13, no. 1, pp. 66-73.
- [23] Shaabana, I.G. and Said, M. (2018). Finite element modeling of exterior beam-column joints strengthened by ferrocement under cyclic loading, *Case Studies in Construction Materials*, vol. 8, pp. 333–346, <https://doi.org/10.1016/j.cscm.2018.02.010>.
- [24] Najafgholipour, M.A., Dehghan, S.M., Dooshabi, A., Niroomandi, A. (2017). Finite Element Analysis of Reinforced Concrete Beam-Column Connections with Governing Joint Shear Failure Mode, *Latin American Journal of Solids and Structures*, vol. 14, pp. 1200-1225, <http://dx.doi.org/10.1590/1679-78253682>.
- [25] Abusafaqa, F. R., Samaaneh, M. A., and Dwaikat, M. B. M. (2022). *Structures*, vol. 36, pp. 979–996.
- [26] Park, R. and Paulay, T. (1975). *Reinforced concrete structures*, John Wiley and Sons, New York.
- [27] Cohn, M. Z. and Bartlett, M. (1982). Computer-simulated flexural tests of partially pre-stressed concrete sections, *ASCE Journal of the Structural Division*, vol. 108, no. 12, pp. 2747–2765, <https://doi.org/10.1061/JSDEAG.0006103>.
- [28] Azizinamini, A., Pavel, R., Hatfield, E., and Gosh, S. K. (1999). Behavior of lap spliced reinforcing bars embedded in high strength concrete, *ACI Structural Journal*, vol. 96, no. 5, pp. 826-836, <https://doi.org/10.14359/737>.
- [29] American Society of Civil Engineers. (2000). FEMA-356 Prestandard and Commentary for the Seismic Rehabilitation of Buildings, prepared for the SAC Joint Venture, Federal Emergency Management Agency, Virginia, Washington, D.C, pp. 3-19 to 3-20.
- [30] Kim, I.H., Kim, J.K. (2004). Seismic Design Strategies and Details Appropriate to Moderate Seismicity Regions, 13th World Conference on Earthquake Engineering, Vancouver, B.C., Canada, August 1-6, paper no. 1420.
- [31] Dietrich, M. Z., Calenzani, A. F. G., Fakury, H. L. (2019). Analysis of rotational stiffness of steel-concrete composite beams for lateral torsional buckling, *Engineering Structures*, Vol. 198, No. 109554, pp. 1-15.

Paper submitted: 29.01.2022.

Paper accepted: 29.03.2022.

This is an open access article distributed under the CC BY 4.0 terms and conditions.